2017

K2 Campaign 5 observations of pulsating subdwarf B stars: binaries and super-Nyquist frequencies

Mike D. Reed
Missouri State University

E. L. Armbrecht
MSU Undergraduate

J. H. Telting

A. S. Baran

R. H. Østensen
Missouri State University

See next page for additional authors

Authors

Mike D. Reed; E. L. Armbrecht; J. H. Telting; A. S. Baran; R. H. Østensen; Pere Blay; A. Kvammen; Teet Kuutma; T. Pursimo; and For complete list of authors, see publisher's website.

K2 Campaign 5 observations of pulsating subdwarf B stars: binaries and super-Nyquist frequencies

M. D. Reed,[1]⋆ E. L. Armbrecht,[1] J. H. Telting,[2] A. S. Baran,[3] R. H. Østensen,[1]
Pere Blay,[2,4,5] A. Kvammen,[2,6] Teet Kuutma,[2] T. Pursimo,[2] L. Ketzer[1]
and C. S. Jeffery[7]

[1]*Department of Physics, Astronomy and Materials Science, Missouri State University, 901 S. National, Springfield, MO 65897, USA*
[2]*Nordic Optical Telescope, Rambla José Ana Fernández Pérez 7, E-38711 Breña Baja, Spain*
[3]*Suhora Observatory and Krakow Pedagogical University, ul. Podchor[ąży ch 2, PL-30-084 Kraków, Poland*
[4]*Instituto Astrofísico de Canarias, Via Lacatea S/N, E-38200 La Laguna, Tenerife, Spain*
[5]*ULL, Avda. Astrofísico Fco. Sánchez S/N, E-38200 La Laguna, Tenerife, Spain*
[6]*Department of Physics and Technology, University of Tromsø, Tromsø 9019, Norway*
[7]*Armagh Observatory, College Hill, Armagh BT61 9DG, UK*

ABSTRACT

We report the discovery of three pulsating subdwarf B stars in binary systems observed with the *Kepler* space telescope during Campaign 5 of *K2*. EPIC 211696659 (SDSS J083603.98+155216.4) is a *g*-mode pulsator with a white dwarf companion and a binary period of 3.16 d. EPICs 211823779 (SDSS J082003.35+173914.2) and 211938328 (LB 378) are both *p*-mode pulsators with main-sequence F companions. The orbit of EPIC 211938328 is long (635 ± 146 d) while we cannot constrain that of EPIC 211823779. The *p* modes are near the Nyquist frequency and so we investigate ways to discriminate super- from sub-Nyquist frequencies. We search for rotationally induced frequency multiplets and all three stars appear to be slow rotators with EPIC 211696659 subsynchronous to its orbit.

Key words: stars: oscillations – subdwarfs.

1 INTRODUCTION

Subdwarf B (sdB) stars are horizontal branch stars, which have shed their outer blanket of hydrogen, exposing their cores for probing. The mechanism for removing the envelope is still uncertain. Proposed mechanisms typically include companion stars (or planets; Han et al. 2002; Geier et al. 2012), which undergo either a common-envelope (CE) phase or Roche lobe overflow. After completion of the CE phase, the sdB star and its companion are typically close, but sufficiently separated to be non-interacting. Stable Roche lobe overflow (Han et al. 2002) results in wide binaries. Another mechanisms for producing sdB stars is white-dwarf (WD) mergers (Webbink 1984), which can produce single sdB stars. The formation channel leaves an imprint on the sdB mass and these factors make sdB stars very important for the study of binary interactions. Other post-CE binaries include neutron stars and WDs, which are often interacting, making those systems complex (Ivanova et al. 2013).

In addition, *how* the two stars interact in order to remove the sdB mass will affect observable properties, such as rotation period (via angular momentum exchange, Kawaler & Hostler 2005),

eccentricity (Vos et al. 2017), and core-envelope mass distributions (via CE ejection efficiency). Since asteroseismology can be used to probe rotation profiles and core and envelope masses, it can be a powerful tool for understanding these processes.

Pulsating subdwarf B (sdBV) stars have been found to pulsate in both gravity (*g*) and pressure (*p*) modes (Kilkenny et al. 1997; Green et al. 2003) with periods of a few hours or a few minutes, for each type, respectively. Amplitudes are typically a few parts-per-thousand (ppt) or less and until the *Kepler* (hereafter *K1*) and *K2* missions, observational mode constraints were difficult to obtain. *K1* and *K2*'s long duration and high-duty-cycle observations provided the breakthrough in correlating pulsations with modes. Asymptotic *g*-mode period spacings (Reed et al. 2011) and rotationally split frequency multiplets (Baran et al. 2012) have been used to identify pulsation modes. Frequency multiplets also measure the rotation period and thus far, *every K1*-observed binary sdBV star is rotating subsynchronously (Pablo, Kawaler & Green 2011; Baran & Winans 2012; Pablo et al. 2012; Telting et al. 2012), though the three hour sdBV+dM binary KIC 9472174 may be an exception (Østensen et al. 2010a). Hybrid pulsators have both *p* and *g* modes, with *g* modes probing deeper into the star, while *p* modes are constrained to the envelope (Charpinet et al. 2000). Hybrid pulsators can then be used to measure any difference in rotation between the

⋆ E-mail: mikereed@missouristate.edu

core and the envelope. To date, hybrid pulsators have revealed two solid-body rotators (Baran et al. 2012; Kern et al. 2017) and two differential rotators (Foster et al. 2015; Baran et al. 2017), with the core rotating slower than the envelope. The long, uninterrupted duration of *K1* and *K2* observations has allowed us to investigate the long-term stability of sdB pulsations. Typically the amplitudes are highly variable and sometimes even the frequencies are variable (Østensen et al. 2014; Kern et al. 2017; Ketzer et al. 2017). For a summary of *K1*-observed sdBV results see Reed & Foster (2014) and for a full review of sdB properties (including some *K1* results), see Heber (2016).

In this paper, we investigate three pulsators from *K2*'s Campaign 5. EPIC 211696659 (hereafter J08360), is identified with SDSS J083603.98+155216.4 (York, Adelman & Anderson 2000) with $g = 15.18$ mag. It was observed as part of the LAMOST survey (Luo et al. 2016), which lists spectroscopic parameters of $T_{\mathrm{eff}} = 27100 \pm 640\,K$, $\log g = 5.419 \pm 0.069$, and $\log y = -2.451 \pm 0.174$, placing it within the *g*-mode instability region. EPIC 211823779 (SDSS J082003.35+173914.2 and hereafter J08200) was determined to be an sdB star with a main-sequence companion from a Sloan survey spectrum. EPIC 211938328 is listed as LB 378 and EGGR 266 in SIMBAD (and hereafter referred to as LB 378) and a BOSS spectrum (Dawson et al. 2013) was obtained by the Sloan Digital Sky Survey (SDSS J083612.02+191755.9; Stoughton et al. 2002). From that spectrum, it was classified as sdB by Carter et al. (2013). These stars were on our *K2* Cycle 1 GO proposal and this paper completes publications of sdBV stars discovered from that proposal (Baran et al. 2017; Jeffery et al. 2017).

2 OBSERVATIONS AND DATA PROCESSING

J08360, J08200, and LB 378 have $K_{\mathrm{p}} = 15.5$, 15.2, and 15.8, respectively, and they were observed by *K2* during Campaign 5 for ≈ 75 d from 2015 April to July, in short-cadence mode, which summed nine images into 58.8 s integrations. We downloaded pixel array files from the Mikulski Archive for Space Telescopes and processed them using both a custom set of programs (Baran et al. 2017) and PYKE programs (Still & Barclay 2012), with the latter only being used for comparison. Our pipeline uses IRAF's DAOFIND package to determine stellar centres for each image and then PHOT is used to extract fluxes with aperture photometry. Drift across pixels, caused by solar pressure and thruster firings, are corrected using our own decorrelation programs. The extracted differential fluxes are normalized and multiplied by 1000 to have units of ppt.

2.1 Pulsation analysis

75 d of near-continuous observations yields a 1/T resolution of 0.155 µHz, which requires a detection threshold in the amplitudes of the Fourier transforms (FT) of 4.3σ (Bevington & Robinson 2003) to ensure that no peaks are likely caused by random noise. To detect periodicities, we follow the same procedures as in our previous papers (see Reed et al. 2016; Ketzer et al. 2017), where we visually find peaks in the FT above the detection limit, examine them in the time domain using sliding FTs (SFTs), and then decide whether the peaks are sufficiently stable to use traditional pre-whitening or fit them using Lorentzians. Only the highest amplitude periodicity and its neighbour in J08200 were sufficiently stable for pre-whitening to be used. In all other cases, we fitted the FT using Lorentzians (except for known artefacts) and use the widths as the frequency uncertainty as it indicates the amount of variability occurring during observations.
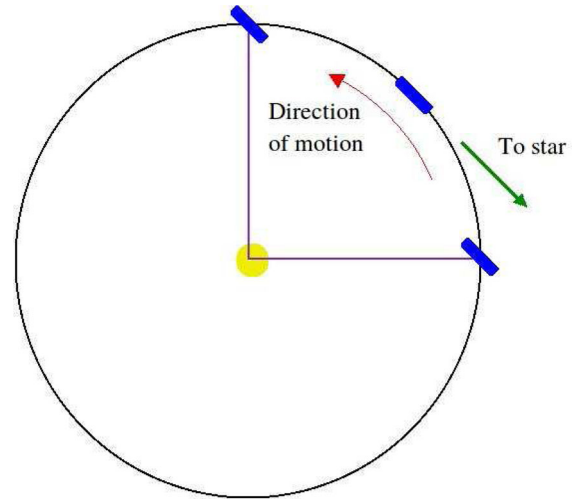


Figure 1. Schematic of the *K2* observing direction.

2.1.1 Super-Nyquist frequencies

For J08200 and LB 378, pulsation frequencies appear on both sides of the Nyquist frequency (see Fig. 6). This is a known issue for *p*-mode sdBV stars as the Nyquist for *K1*'s data is near 8497 µHz and super-Nyquist frequencies were previously detected in the sdBV star KIC 10139564 (Baran et al. 2012). *K1* observed over three orbits, so the frequency drift could easily be observed in the Nyquist and long-cadence (LC) artefacts. Additionally, frequency multiplets appeared smeared in the reflection across the Nyquist, providing a method for determining whether the intrinsic frequency was super- or sub-Nyquist.

The observing configuration is different for *K2* than it was for *K1*. During *K1* the telescope was pointed roughly perpendicular to the spacecraft motion (see fig. 2 of Murphy et al. 2013), whereas during *K2* the spacecraft is rear-facing directly along the ecliptic (Fig. 1). Each campaign is designed so the telescope is aligned tangent along its orbit near to the midpoint of the observing run. Two effects are of potential interest: a slight change in brightness caused by spacecraft motion (Doppler boosting) and a shifting Nyquist frequency. The time stamps of the intregrated images are converted into BJD, but the integrations themselves begin and end in the spacecraft's time frame. Since the spacecraft is in motion, there is the well-known Doppler boosting that occurs. Normally, we measure this due to stellar motion, but telescope motion will cause it as well. Since we normalize fluxes (to $\Delta I / \langle I \rangle$ where $\langle I \rangle$ is the average flux) piece-wise using five day chunks, this effect is removed.

Murphy et al. (2013), and see also Baran et al. (2012), describe how the full-orbit motion of the *K1* spacecraft, and implied phase-shifts due to differences in light-travel time, results in different multiplet structures at both sides of the Nyquist frequency, and how these particular features help in identifying the true frequencies among those that are duplicated and folded around the Nyquist frequency. Those authors describe the effects in Fourier space in the case of data coverage as long as a full *K1* orbit (approximately one year) or longer. Here, we discuss how the structures around Fourier peaks arise for *K2* campaigns, which span only three months of data, aiming to use these particular structures in Fourier space to identify true pulsation frequencies.

To investigate this, we examined how a signal generated in the space telescope's reference frame would appear in the barycentric frame. We generated a simulated signal as a sinusoid of constant
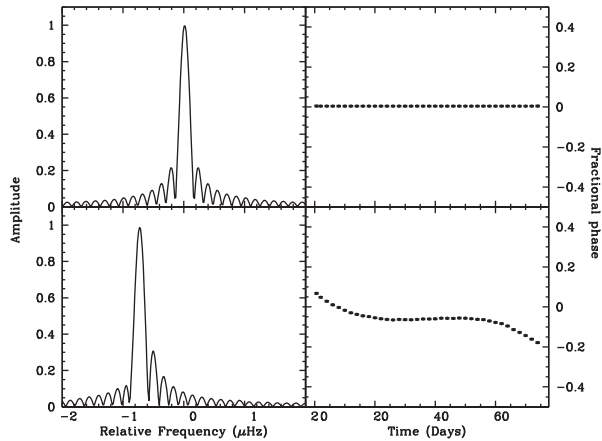
Figure 2. Simulations of a periodic signal in the spacecraft's reference frame (top panels) and shifted to the barycentre (bottom panels). Left-hand panels show FTs. For the top left-hand panel, this is also known as a window function as it shows the effects of sampling gaps in the data (the sidelobes). The right-hand panels show fractional phases (in bins of two days) of the main peak of the FTs in the appropriate reference frame.

frequency (around 7950 µHz where we are interested), amplitude, and phase, sampled every 58.85 s (the short cadence, SC) in the spacecraft reference frame. We then extracted the barycentric corrections from the Campaign 5 images and added these to the signal's times. The results are shown in Fig. 2. With the signal in the spacecraft reference frame (top panels), the small aliasing is symmetric and the phase of the variations is constant. In the shifted reference frame (bottom panels), the frequency is shifted by the spacecraft motion, the aliasing pattern is asymmetric, the amplitude is slightly reduced, and the phases (calculated as time of first maximum divided by the period and offset to be around zero) show deviations of ∼20 per cent. The shifting of the observing times to the barycentre has caused some power of the variations to be shifted to the side lobes. Signals external to our Solar system are corrected by translating to the barycentric frame, but signals at rest within the spacecraft's reference frame will be affected. So reflections across the Nyquist, which are signals external to our Solar system combined with one from the spacecraft, will obtain the features of the bottom panels of Fig. 2.

As such, these tools can be used to distinguish intrinsic from reflected when pulsations are observed across the Nyquist frequency. If the signal-to-noise ratio (S/N) is high enough, this amplitude change and asymmetry of aliasing could be detected (see for example in Fig. 7). Likewise, if the pulsation phases are constant, the shift imposed by the time stamps could be detected.

3 RESULTS OF FOURIER ANALYSES

3.1 J08360

The FT of J08360 is provided in Fig. 3 and the fitted periodicities are listed in Table 1. The detection limit for the full data set is 0.077 ppt. The highest amplitude variability occurs at 3.67 µHz, which we know corresponds to a binary period (see Section 3.1) and is caused by Doppler boosting. That peak is both amplitude and phase stable over the course of the observations. All other variabilities are associated with stellar pulsations and shown in Fig. 4, which has SFTs in the top panels with amplitudes given in σ. Each FT spans five days with each subsequent FT stepped by two
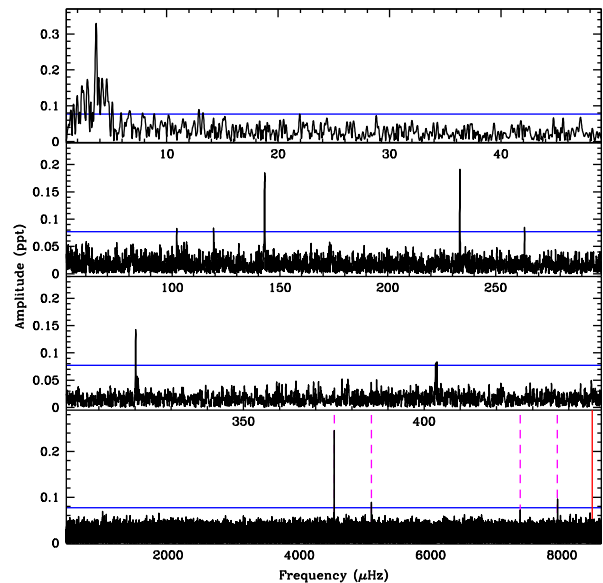
Figure 3. Fourier transform of J08360 up to the Nyquist frequency (red line). The horizontal line indicates the 4.3σ detection limit and the vertical dashed lines indicate known spacecraft artefacts.

days. *None* of the pulsations persist at observable levels over the entirety of the observations. The lower panels show the same region, but for the entire data set. Table 1 lists amplitudes from the full data set, even though some are below the detection threshold as they are of significant levels in subset FTs (even with correspondingly higher σ).

With the discovery of a 3.1 d binary period (Section 3.1 with the orbital parameters provided in Table 5), if J08360 is tidally locked, it is well suited for detecting frequency multiplets caused by rotation. Frequencies should be separated by $\Delta\nu_{n,\ell,m} = \Delta m \Omega (1 - C_{n,\ell})$, where Ω is the orbital frequency (3.67 µHz) and $C_{n,\ell}$ is the Ledoux constant estimated as $1/[\ell(\ell + 1)]$ for g modes (Aerts, Christensen-Dalsgaard & Kurtz 2010). For $\ell = 1$, we should see triplets with frequencies separated by 1.84 µHz ($>11 \times$ the temporal resolution), and for $\ell = 2$, we should observed quintuplets with frequencies separated by 3.06 µHz, both of which are easily resolved in *K2* data. However, we detect no such multiplets. The lack of multiplet splittings ≥ 1.84 µHz must mean that J08360 rotates subsynchronous to its binary period and is not tidally locked. There is one marginally resolved multiplet in Table 1. f8–f10 forms a triplet with separations of 0.198 and 0.195 µHz. If this were an $\ell = 1$ triplet, it would indicate a rotation period of 30 d. If it were $\ell = 2$ with Δm of 1 or 2, the rotation period would be 50 or 99 d, respectively. All of these solutions are substantially longer than the orbital period, and so also indicate J08360 to have subsynchronous rotation.

Other than f8–f10, there are other peaks, which appear forked, but not fully resolved (indicated in Fig. 4), yet when we look at the frequency difference in the peaks, they should be. Their splittings are slightly (<0.02) larger, but similar to those of f8–f10, indicating a similar source. There are several possible explanations why the peaks are not fully resolved, the most likely being that the amplitudes are rarely excited to detectable levels. *If* they are multiplets, which are poorly resolved because of pulsation phase interactions (Aerts et al. 2010), and *if* their common separations indicate they are the same modes, then as $\ell = 1$ multiplets, they indicate a rotation period of 28.4 ± 1.4 d. If they are $\ell = 2$ with Δm of 1 or 2, the rotation period would be 47.3 ± 2.3 or 94.6 ± 4.5. Any of

Table 1. Periods detected for J08360. Column 1 provides an ID, columns 2 and 3 provide frequencies and periods with errors (Lorentzian widths) in parentheses. Column 4 lists the amplitude and Column 5 lists the corresponding S/N. Column 6 lists the mode degree with columns 7 and 8 listing relative radial indices. Columns 9 and 10 list the deviation from the asymptotic sequence. No peaks attributed to spacecraft artefacts are listed in this table. Note: [a] These periodicities have low S/N in our final processing, but match asymptotic spacing and so were retained in our table. [b] This frequency was fitted using non-linear least-squares so the errors are from that fit and this period is reported in days.

ID	Frequency (μHz)	Period (s)	Amplitude (ppt)	S/N	ℓ	$n_{\ell = 1}$	$n_{\ell = 2}$	$\delta P / \Delta \Pi_1$ per cent	$\delta P / \Delta \Pi_2$ per cent
fA[b]	3.670 (4)	3.154 (4) d	0.33 (1)						
f1[a]	119.25 (05)	8385.9 (3.4)	0.075	4.2	1/2	36	63	8.0	5.3
f2[a]	119.45 (05)	8371.6 (3.7)	0.056	3.1	1/2	36	63	1.7	-5.6
f3	142.81 (13)	7002.2 (6.2)	0.120	6.7	1	30		-1.5	
f4	143.03 (12)	6991.5 (5.8)	0.122	6.8	1	30		-6.1	
f5	233.41 (11)	4284.3 (1.9)	0.188	10.4	1	18		1.5	
f6	263.42 (12)	3796.2 (1.7)	0.077	4.3	1/2	16	28	-13.4	5.2
f7	320.17 (08)	3123.3 (.8)	0.141	7.8	1/2	13	23	-9.8	-7.9
f8	403.13 (06)	2480.6 (.4)	0.079	4.4	1/2	10	18	7.1	1.9
f9[a]	403.33 (05)	2479.4 (.3)	0.072	4.0	1/2	10	18	6.6	1.0
f10[a]	403.52 (05)	2478.2 (0.3)	0.074	4.1	1/2	10	18	6.0	0.1

these possibilities still indicate rotation periods much longer than the binary period. We list these multiplets in Table 1 as if they are separate frequencies, but strongly caution that it is possible that all of them are single frequencies, which are split because of amplitude and/or frequency variations.

J08360 does not have a rich pulsation spectrum, and so it is not difficult to assign modes to the periodicities using asymptotic period spacings. Excluding the multiplets, there are only six independent frequencies and differencing the periods easily shows multiples near the known sdBV $\ell = 1$ asymptotic value around 250 s. The smallest spacing is 488 s, which we consider to be $\Delta n = 2$. There are two other spacings between 640 and 680 s, which we presume are $\Delta n = 3$, with the remaining two spacings being quite large. If our Δns are correct, these are spacings of 244, 214, and 224 s, providing a starting point for a sequence. We use a standard Kolmogorov–Smirnov (KS) test to search for equal period spacings, with the result shown in Fig. 5. The most significant (deepest) trough is forked, which is fairly common for this test, and spans 5 s centred at 227 s. With this as guidance, we could assign asymptotic overtones, n, to the remaining periods. A linear regression fit provides a solution of 227.05 ± 0.056 s, which we assign as the $\ell = 1$ asymptotic sequence. This is shown in green in Fig. 5 and falls right in the middle of the deepest trough.

The $\ell = 2$ asymptotic spacing should be $1/\sqrt{3}$ of the $\ell = 1$ sequence. We produced a model sequence from this relation and looked for matching with observed periods. Quite surprisingly, four of the six periods fit the $\ell = 2$ sequence as well. There is no hint of this sequence in the KS test, which is marked with a magenta line in Fig. 5. Since we cannot distinguish between them, we list both mode identifications in Table 1

3.2 J08200

We only detect p-mode pulsations in J08200's temporal spectrum (shown in the top panel of Fig. 6), with symmetric peaks on both sides of the Nyquist. The detection limit is 0.049 ppt and we detect 40 periodicities above that level, including some known spacecraft artefacts. These are provided in Table 2. Excluding known artefacts and their reflections, we detect 16 periodicities attributable to pulsations with a similar number of reflections.

The known LC artefacts and their reflections are labelled as such in Table 2, but the pulsations need to be distinguished from their re-

flections. To do so, we used the evidence from our simulation shown in Fig. 2. The SFTs for J08200 indicate the pulsations are amplitude variable, so we do not attempt to measure phases, but rather concern ourselves with asymmetric frequency peaks and relative amplitudes. The highest amplitude peaks appear as multiplets, and so the best example is the well-separated frequency f05 and its super-Nyquist counterpart. This is shown in Fig. 7 with one peak having a symmetric alias pattern (top panel) and the other an asymmetric pattern (bottom panel) and a slightly lower amplitude, just like the simulation. Using this methodology, we distinguished intrinsic from reflected frequencies.

Even this methodology has complications for J08200 as regions appear mixed above and below the Nyquist, as shown in Figs 8 and 9. In the former, the regions around 5332 and 11 661 μHz are shown. The highest amplitude peak (f16) is in the super-Nyquist region and, as it should, its reflection has a higher amplitude neighbouring alias. However, the peak at 5332.73 μHz (f01) has a higher amplitude in the sub-Nyquist region and the super-Nyquist reflection (at 11661.5 μHz) shows an asymmetry in its structure. So in this case, we presume the pulsation is the sub-Nyquist one (f01). So this apparent triplet is in reality two very well-separated individual peaks (at 5332.73 and 11660.98 μHz), one of which is split because of amplitude and/or phase variability. In Fig. 9 the peak at 7333 μHz (f12) is above the detection limit and its reflection is just below, while next to f12 is a peak just below the detection limit in the sub-Nyquist, but is above the detection limit in the super-Nyquist region (f14). In both of the regions, we assign some of the pulsations as sub-Nyquist and others as super-Nyquist.

While those two sets of frequencies are not intrinsic multiplets, other regions have them. We detect four different multiplets each with separations that increase with increasing frequency. f03–f04, f06–f07, f08–f10, and f11–f12 are split by 0.541, 0.924, 2.165, and 3.062 μHz, respectively. These splittings are surprisingly all close to multiples of 0.5 μHz and if this were the intrinsic splitting, then they would be $\Delta m = 1, 2, 4,$ and 6, respectively, making the modes $\ell = 1, 1$ or 2, 2, and 3, respectively. We think this interpretation unlikely. We were able to pre-whiten both the highest amplitude frequency f06 and its neighbour f07, indicating these were stable, and so their separation is the most secure. So we presume the intrinsic splitting to be near 1.0 μHz with f03–f04 either caused by chance of two single periodicities or amplitude and/or phase variability. Hence we assume f06–f07 is an $\ell = 1$ doublet,
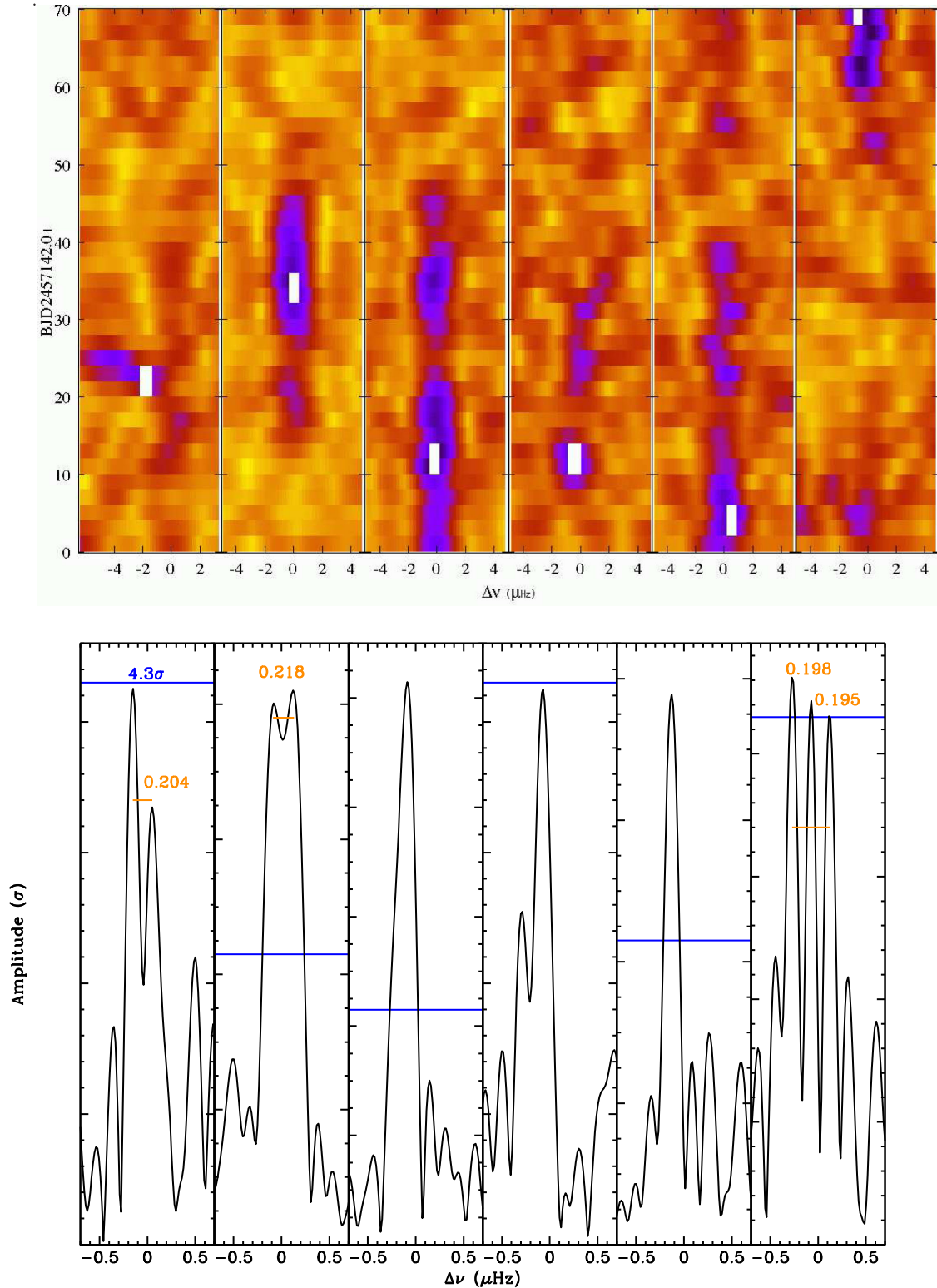
Figure 4. Top panels: sliding FT of the pulsations in J08360. Frequency is on the abscissa and time on the ordinate with colour indicating the amplitude, in σ. Frequency centres are (from the left- to right-hand side) 119.35, 142.9, 233.4, 263.4, 320.2, and 403.4 μHz. The amplitudes are scaled such that the white pixels are just above (from the left- to right-hand side) 4.2, 6.5, 4.9, 3.2, 3.7, and 3.9σ. Bottom panels: same frequency range as the top panels, but showing FTs of the full data set. Horizontal (blue) lines indicate the 4.3σ detection limit in all panels and so indicate the scaling for each panel. Numbers within panels are the frequency splittings.
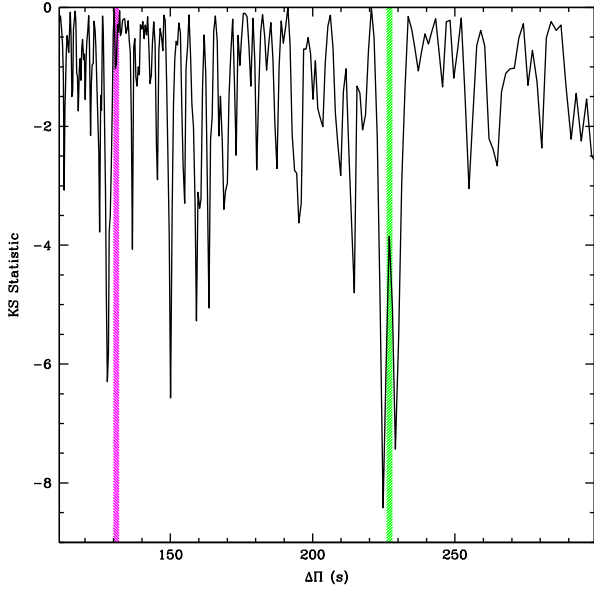
Figure 5. KS test distribution of period spacings. Shaded green and magenta regions indicate the possible $\ell = 1$ and 2 spacings.
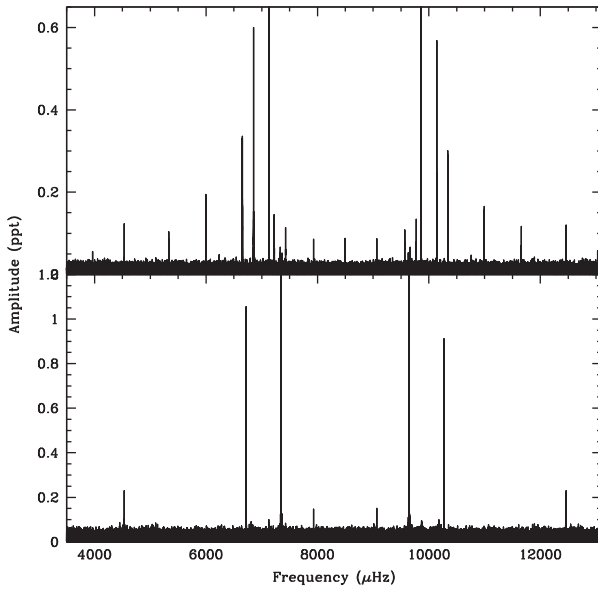
Figure 6. The *p*-mode pulsators J08200 (top panel) and LB 378 (bottom panel) showing both the sub and super-Nyquist regions. The highest amplitude peak has been truncated to better show the lower amplitude pulsations.

f08–f10 is an $\ell = 2$ doublet with $\Delta m = 2$, and f12–f13 is a possible doublet with $\Delta m = 3$, and the average frequency splitting is $1.01 \pm 0.08\,\mu$Hz. As all we detect are doublets, other mode identification interpretations are possible.

3.3 LB 378

We detected a total of 23 frequencies above the detection limit of 0.10 ppt in LB 378's FT and these are provided in Table 3. Of these, six are known LC artefacts and their Nyquist reflections, leaving eight as intrinsic frequencies with eight Nyquist reflections. In this case, we find all pulsation frequencies to be sub-Nyquist in a fairly narrow range between 6721 and 7347 μHz (136–149 s). In such a narrow range, these likely belong to the same radial overtone, and

Table 2. Periods detected for J08200. Column 1 provides an ID with f indicating a frequency considered intrinsic to the star, R a reflection across the Nyquist (number indicates frequency it is reflected from), A are known spacecraft-induced artefacts, and AnR indicates reflections of artefact n. Columns 2 and 3 provide frequencies and periods with errors (Lorentzian widths) of pulsations in parentheses, Column 4 lists amplitudes, and Column 5 lists the corresponding S/N. ^{a} indicates frequencies fitted using non-linear least-squares. All others were fitted using Lorentzian functions.

ID	Frequency (μHz)	Period (sec)	Amplitude (ppt)	S/N	ℓ, m
A1	3965.35	252.185	0.069	4.9	
A2	4531.82	220.662	0.123	10.7	
f01	5332.73	187.521	0.080	7.0	
R16	5333.28	187.502	0.103	9.0	
f02	5999.35 (23)	166.685 (6)	0.194	16.9	
f03	6654.55 (18)	150.273 (4)	0.336	29.3	
f04	6655.10 (17)	150.261 (4)	0.330	28.8	
f05	6851.87 (8)	145.946 (2)	0.600	52.30	
f06^a	7131.9538 (5)	140.21403 (1)	2.052	179.0	1,0
f07^a	7132.8778 (17)	140.19587 (3)	0.592	51.7	1,1
f08	7222.71 (8)	138.452 (2)	0.145	12.7	2,0
f09	7223.50 (12)	138.437 (2)	0.082	7.1	–
f10	7224.87 (10)	138.411 (2)	0.064	5.6	2,2
R15	7227.02 (10)	138.37 (2)	0.064	5.5	
f11	7330.41 (8)	136.418 (1)	0.066	5.7	≥2
f12	7333.47(8)	136.361 (1)	0.053	4.6	≥2
A3	7364.15	135.793	0.052	4.5	
f13	7427.25 (24)	134.639 (4)	0.114	9.9	
A4	7930.67	126.093	0.086	7.5	
A5	8497.17	117.686	0.088	7.6	
A4R	9063.61	110.331	0.087	7.6	
R13	9567.04	104.526	0.108	9.4	
A3R	9630.14	103.841	0.052	4.6	
f14	9660.59 (8)	103.513 (1)	0.054	4.7	
R11	9663.89	103.478	0.066	5.8	
f15	9767.25	102.383	0.066	5.8	
R10	9769.42	102.36	0.060	5.2	
R09	9770.78	102.346	0.080	6.9	
R08	9771.57	102.338	0.134	11.7	
R07	9861.20	101.408	0.290	25.3	
R06	9862.33	101.396	1.954	170.4	
R05	10142.19	98.5981	0.247	21.5	
R05	10142.42	98.5958	0.568	49.5	
R04	10339.74	96.7142	0.301	26.2	
R03	10340.06	96.7112	0.103	9.0	
R02	10994.72	90.9528	0.165	14.4	
f16	11660.98 (8)	85.7561 (6)	0.117	10.2	
R01	11661.54	85.752	0.065	5.6	
A2R	12462.46	80.241	0.120	10.5	
A1R	13028.94	76.7522	0.057	5.0	

indeed there are really only two regions of power, and these are shown in Fig. 10. The SFT near 6721 μHz shows obvious signs of beating and the FT is split into a frequency-symmetric triplet, though the central, high-amplitude peak is itself asymmetric. The pulsations near 7345 μHz are more complex. The main, highest amplitude peak is split into two. The reason for this is obvious in the SFT as the amplitude greatly diminishes in the middle of the run. We do not interpret this splitting as two closely spaced frequencies, but consider it most likely due to a change in pulsation phase by nearly 180°. The two outer peaks show the expected beat pattern to the central peaks, and so these are likely intrinsic to the star, rather than aliases, and this is our interpretation. This region is thus
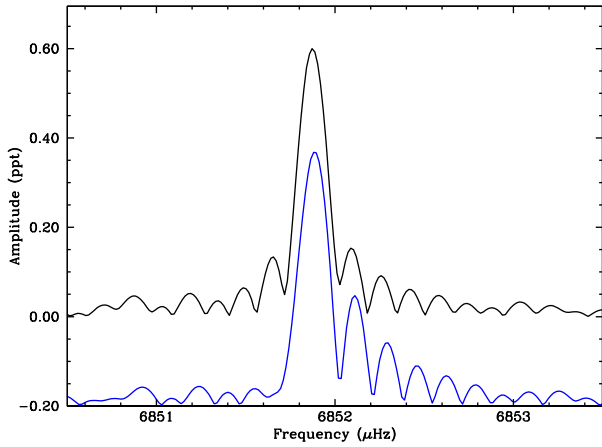
Figure 7. Example of reflected frequency across the Nyquist (J08200). The top line indicates the original frequency and aliases while the bottom line (offset by 0.2 ppt) is the reflection across the Nyquist.
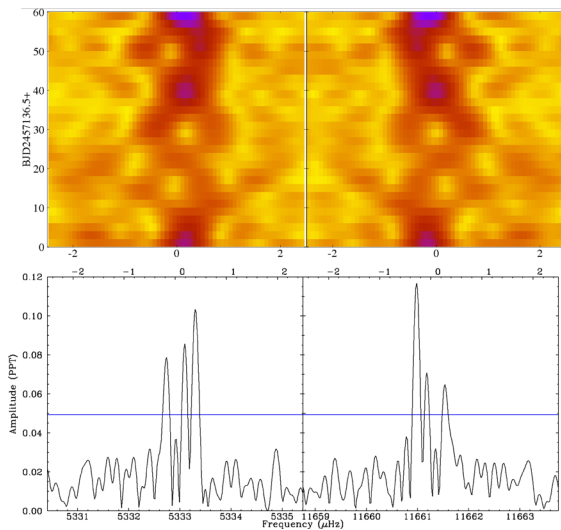

Figure 8. Sub- and super-Nyquist regions for J08200 of the same variations across the Nyquist frequency. Top panels show SFTs covering 15 d of data with 2 d steps. Bottom panels show FTs of the complete data set.

a triplet, with frequency splittings slightly over twice that of the 6721 μHz triplet, and a single (perhaps radial) frequency.

With these interpretations, we have detected two multiplets with an average $\Delta m = 1$ splitting of 0.538 ± 0.014 μHz and single periodicities at 7337.80 and 7345.31 μHz. Everything else is either an artefact or a reflection across the Nyquist.

4 SPECTROSCOPIC OBSERVATIONS AND ANALYSES

As part of our follow-up spectroscopic survey (Telting et al. 2014), low-resolution spectra (R ~2000) have been obtained for all three stars using the 2.56 m Nordic Optical Telescope (NOT) with ALFOSC, grism #18 and a 0.5 arcsec slit. Observations from before 2016 April were obtained with CCD#8, with approximate wavelength range 353–530 nm, while newer observations were obtained with CCD#14 giving an approximate wavelength range 345–535 nm. For either CCD the resulting resolution based on the width of arc lines is 2.2 Å.
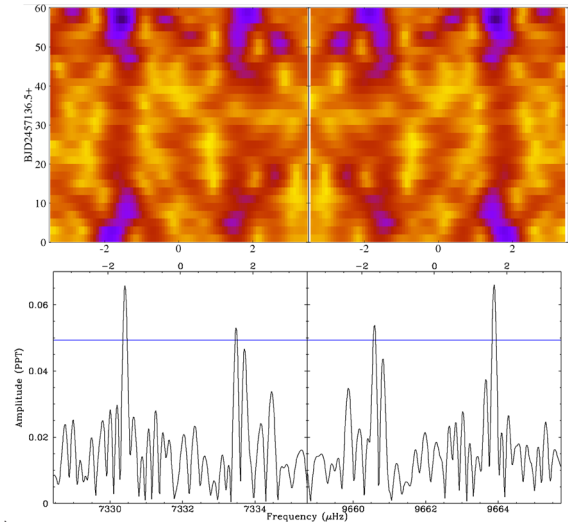

Figure 9. Same as Fig. 8 for another example of mixed sub- and super-Nyquist pulsations in J08200.

Table 3. Periods detected for LB 378. Columns are as in Table 2.

ID	Frequency (μHz)	Period (s)	Amplitude (ppt)	S/N	ℓ, m
A1	4531.82	220.662	0.23	20.0	
f1	6721.33 (7)	148.780 (2)	0.50	43.2	1,−1
f2	6721.86 (10)	148.768 (2)	1.05	92.0	1,0
f3	6722.38 (7)	148.757 (2)	0.20	17.3	1,1
f4	7337.78 (8)	136.281 (2)	0.12	10.8	–
f5	7344.00 (9)	136.166 (2)	0.92	80.1	2,−2
f6	7345.11 (5)	136.145 (1)	2.36	103.2	2,0
f7	7345.31 (5)	136.141 (1)	2.95	131.2	–
f8	7346.21 (9)	136.125 (2)	0.76	66.7	2,2
A2	7364.15	135.793	0.12	10.9	
A3	7930.64	126.093	0.15	12.8	
A3R	9063.65	110.331	0.15	13.1	
A2R	9630.12	103.841	0.11	9.5	
R8	9648.08	103.648	1.02	88.8	
R7	9648.77	103.64	2.00	174.2	
R6	9649.17	103.636	1.74	152.0	
R5	9650.27	103.624	0.96	83.6	
R4	9656.30	103.559	0.10	9.1	
R3	10271.87	97.3532	0.26	22.8	
R2	10272.21	97.35	0.47	40.9	
R2	10272.45	97.3478	0.91	79.5	
R1	10272.94	97.3431	0.44	38.2	
A1R	12462.47	80.2409	0.23	20.0	

The spectra were homogeneously reduced and analysed. Standard reduction steps within IRAF include bias subtraction, removal of pixel-to-pixel sensitivity variations, optimal spectral extraction, and wavelength calibration based on helium arc-lamp spectra. The target spectra and the mid-exposure times were shifted to the barycentric frame of the Solar system. For radial velocity (RV) determinations, the spectra were normalized to place the continuum at unity by comparing with a model spectrum for a star with similar physical parameters, as we find for the target (see Section 3.1). Radial velocities were derived with the FXCOR package in IRAF. The RVs were adjusted for the position of the target in the slit, judged from slit images taken just before and after the spectral exposure.

A large fraction of sdB stars are found in binaries with a main-sequence companion. Lisker et al. (2005) found that in a sample
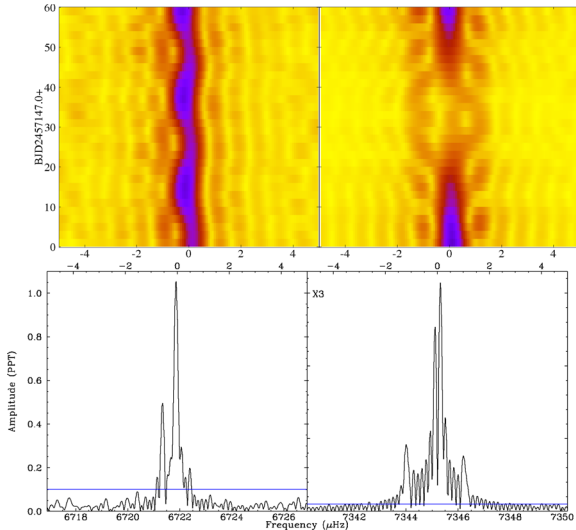
Figure 10. Two pulsations regions for LB 378. Top panels show SFTs with amplitudes in σ while bottom panels show FTs of the entire data set with amplitudes in ppt. Horizontal blue line is the detection limit.

of high-resolution spectra of 76 sdBs observed with VLT/UVES, 24 showed signatures of a companion of spectral class F–K, none of which showed any detectable RV variability. Such systems are expected to form via stable Roche lobe overflow, which will produce orbits with periods of hundreds of days. After Deca et al. (2012), first solved the orbit of the sdB+K binary PG 1018-047, revealing a period of 750 d, patient monitoring by Vos et al. (2017) has reliably solved the orbits of a total of 11 systems spanning a period range of 734–1262 d and MS masses between 0.67 and 1.31 M$_\odot$. Since the absolute magnitude of an extended horizontal branch star is roughly the same as a solar type MS stars, these stars appear as double lined spectroscopic binaries with very different temperatures. But since the RV amplitudes are very low (between 2 and 7 km s^{-1}), solving these systems is very challenging.

The spectra of J08200 and LB 378 include Ca lines indicative of main-sequence companions. To characterize the nature of the companions a 'by-eye' deconvolution was completed. They are described in the pertinent sections for each star below.

4.1 J08360

From 2015 November through 2016 January, we obtained 21 spectra of J08360. Exposure times were 900 s for the first eight spectra, and 600 s for the rest. See Table 4 for an observing log. The spectra have S/N ranging from 28 to 90.

For J08360, we used the H β, H γ, H δ, H ζ, and H η lines to determine the RVs, and used the spectral model fit (see next section) as a template. See Table 4 for the results, with errors in the radial velocities as reported by FXCOR. After shifting the spectra according to the FXCOR RVs to correct for the orbit, another FXCOR iteration revealed RV residuals on the order of 4 per cent of the first-found values. We added the RV results of the two iterations, and adopt the FXCOR errors of the last iteration in our orbit fit.

Assuming a circular orbit, and discarding the one outlier, we find an orbital period of 3.1604(15) d, with a RV amplitude of 67.0(2.6) km s^{-1} for the subdwarf. From the RV amplitude, we calculate a Doppler-boosting light-curve amplitude of 0.31 ppt, and both this and the period match those found from the light curve. The binary-system velocity is found as 24.2(1.6) km s^{-1}. See

Table 4. Spectroscopic observations of J08360.

| BJD	Int. time (s)	S/N	RV (km s^{-1})	Error (km s^{-1})
2457332.61880	900	60.3	44.5	11.4
2457332.69313	900	72.7	21.3	3.8
2457332.74848	900	68.9	17.4	5.3
2457333.66468	900	89.7	− 35.3	4.8
2457333.73411	900	68.3	− 31.4	5.6
2457334.66660	900	84.8	77.0	6.7
2457334.73371	900	78.1	82.6	6.5
2457334.76740	900	77.1	91.5	5.2
2457341.62850	600	27.9	107.1	17.6
2457341.70167	600	32.7	67.2	17.3
2457367.62003	600	46.4	− 8.0	7.7
2457367.78625	600	52.8	− 29.7	8.7
2457397.48993	600	66.4	23.6	7.8
2457397.65381	600	66.6	38.8	6.9
2457397.78128	600	60.2	65.1	11.9
2457398.56795	600	66.4	76.4	6.6
2457398.68660	600	73.8	54.6	6.6
2457400.44730	600	33.0	3.9	13.4
2457400.60808	600	58.7	25.6	5.0
2457413.48118	600	44.2	53.5	11.4
2457413.69024	600	29.6	55.1	13.4

Table 5. Summary of spectroscopic and binary properties of J08360.

Property	Value	Comments
$T_{\rm eff}$	27570(300) K	Combined spectrum
log g	5.70(0.03) dex	Combined spectrum
log (n(He)/n(H))	−2.52(0.08) dex	Combined spectrum
γ	24.2(1.6) km s^{-1}	
Period	3.1604(15) d	RVs, circular orbit
K	67.0(2.7) km s^{-1}	RVs, circular orbit
Reduced χ^2 of the fit	1.10	RVs, circular orbit
Fit RMS	8.1 km s^{-1}	RVs, circular orbit
e	0.07(7)	RVs, non-circular-orbit fit
$A_{\rm Doppler}$	0.31 ppt	K, B=1.40 (sdB+WD beaming factor, Telting et al. 2012),
$(a_1 + a_2)_{\rm min}$	8.7 R$_\odot$	$i = 90°$, $M_{\rm sdB} = 0.47$ M$_\odot$
$(M_2)_{\rm min}$	0.43 M$_\odot$	$i = 90°$, $M_{\rm sdB} = 0.47$ M$_\odot$
$i_{\rm max}$	89°	No observed eclipses.
$(a_1 + a_2)_{\rm canonical}$	9.3 R$_\odot$	$M_{\rm sdB} = 0.47$ M$_\odot$, $M_{\rm WD} = 0.60$ M$_\odot$
$i_{\rm canonical}$	54°	$M_{\rm sdB} = 0.47$ M$_\odot$, $M_{\rm WD} = 0.60$ M$_\odot$
Period	3.154(4) d	Light-curve fit
$A_{\rm Doppler}$	0.33(1) ppt	Light-curve fit

Table 5 for the complete parameter listing. The radial velocities and the derived solution are shown in Fig. 11. When fitting an eccentric RV curve, the eccentricity is fit as $e = 0.07(7)$. We thus use a circular orbit throughout this paper.

Assuming a canonical sdB mass of M$_1$ = 0.47 M$_\odot$, we find that M$_2 >$ 0.43 M$_\odot$, and $a_1 + a_2 >$ 8.7 R$_\odot$. There is no hint of any MS star earlier than M2 in the ALFOSC spectra. This implies that M$_2$ is likely a WD. The observed RV amplitude of 67 km s^{-1}, together with a Doppler-beaming factor of 1.4 that is expected for *K1* observations of a sdB+WD binary (Telting et al. 2012), leads to an expected Doppler-beaming amplitude of 0.31 ppt, which is very close to the observed 0.33(1) (see Table 5 below). Using a canonical
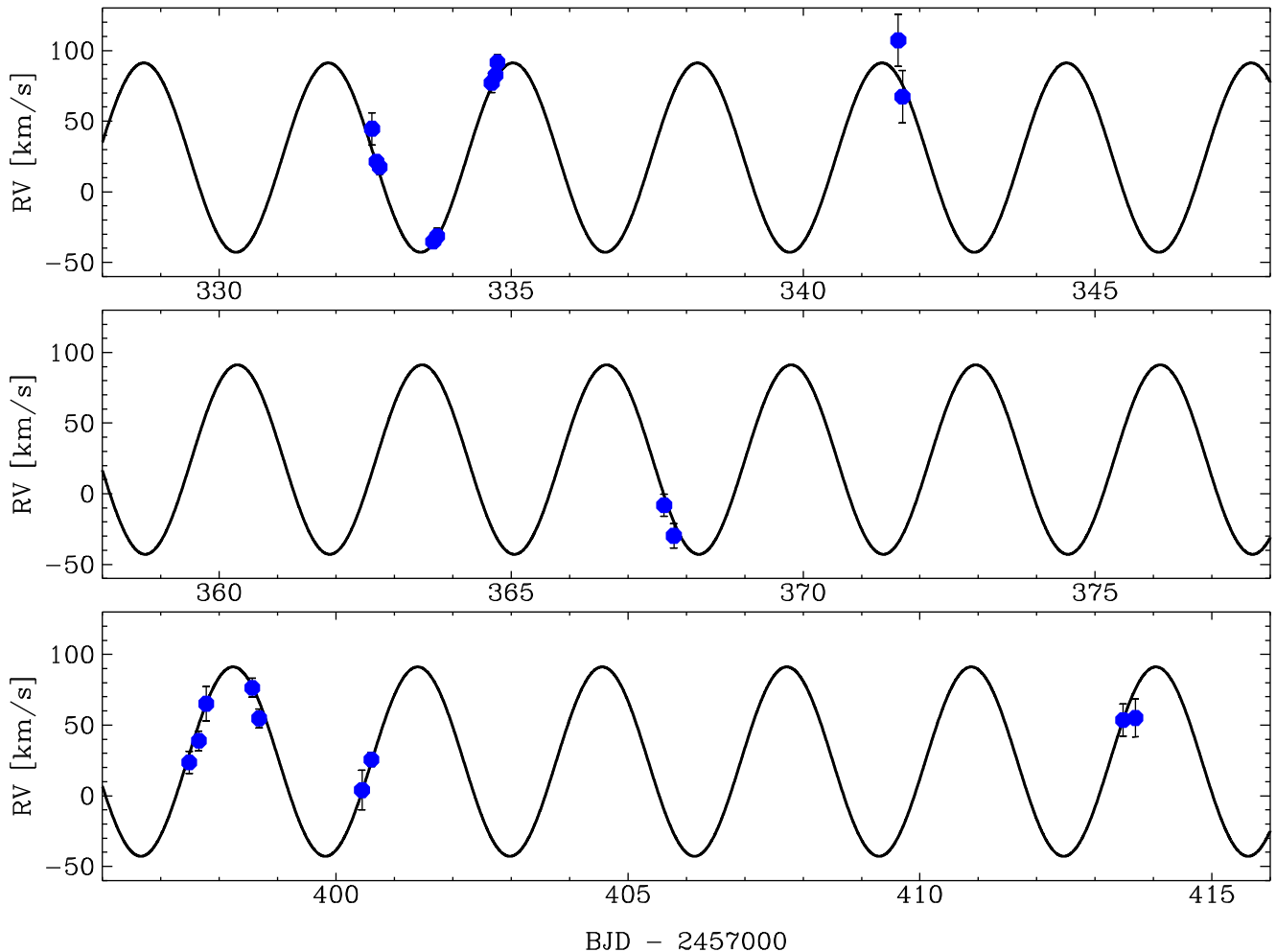
Figure 11. Radial velocities of J08360. The solid line is the fit for the orbital solution, assuming a circular orbit.

WD mass of $M_2 = 0.6 \, M_\odot$ and $M_1 = 0.47 \, M_\odot$, the inclination is required to be the very acceptable $i = 54°$.

We used the mean of all spectra, after shifting each to remove the orbit, and with final S/N ∼ 240, to obtain a high S/N determination of the atmospheric parameters of J08360. We determined $T_{\rm eff}$ and log g (Table 5) from the mean spectrum using the H/He LTE grid of Heber, Reid & Werner (1999) for consistency with Østensen et al. (2010b). We used all the Balmer lines from H β to H14 and the four strongest He I lines for the fit. The errors listed on the measurements are the formal errors of the fit, which reflect the S/N of the mean spectrum. These values and errors are relative to the LTE model grid and do not reflect any systematic effects caused by the assumptions underlying those models.

4.2 J08200

For RV monitoring, 15 spectra of J08200 were obtained between 2015 November and 2017 January. Exposure times ranged from 720 to 1 500 s and the spectra have S/N ranging from 41 to 88. For spectral decomposition, we obtained wide-slit low-resolution spectra with ALFOSC at the NOT on 2016 December 14, using grisms 18, 19, and 20, with dispersions of 0.9, 1.2, and 2.2 Å, respectively. The spectra were fluxed using GD71 as a flux standard, and we used the GD71 model of Moehler et al. (2014) as a flux guide. The combined spectrum spans the entire optical wavelength range.

The composite spectrum of J08200 is complex, as narrow lines in all regions are dominated by the F star, and separating the components for individual RV measurements is difficult. In particular, the Balmer lines have significant contributions from both stars. In an attempt to separate the individual velocities of both stars, radial velocities for the sdB star were determined using H β and H γ, while for the F star metal-line regions avoiding the Balmer lines (415–430, 438–445, 449–482, 490–505 nm) were used. For the cross-correlation, the average of all spectra was used as a template.

In Fig. 12, we show these RV measurements, and it is obvious that we cannot determine the orbit from these low-resolution spectra. We also plot the orbital-RV difference for the two sets. The standard deviation of the two sets of RV measurements is 7 km s^{-1} for both, and is 8 km s^{-1} for the difference of the two sets (see top panel of Fig. 12). Such standard deviations are typical for what we can achieve with our instrumental setup, see for instance the RMS of the orbit fit of J08360 as comparison (Table 5).

Hence we either did not separate the velocities of the two components, or the orbital velocities are so small that we cannot measure them. We can exclude an orbital RV amplitude larger than 10 km s^{-1} for the F star, but can put no constraints on those of the sdB star. An appropriate sdB model spectrum was used to measure an absolute RV of $\gamma = 28.6 \pm 3.7$ km s^{-1} for this binary system.
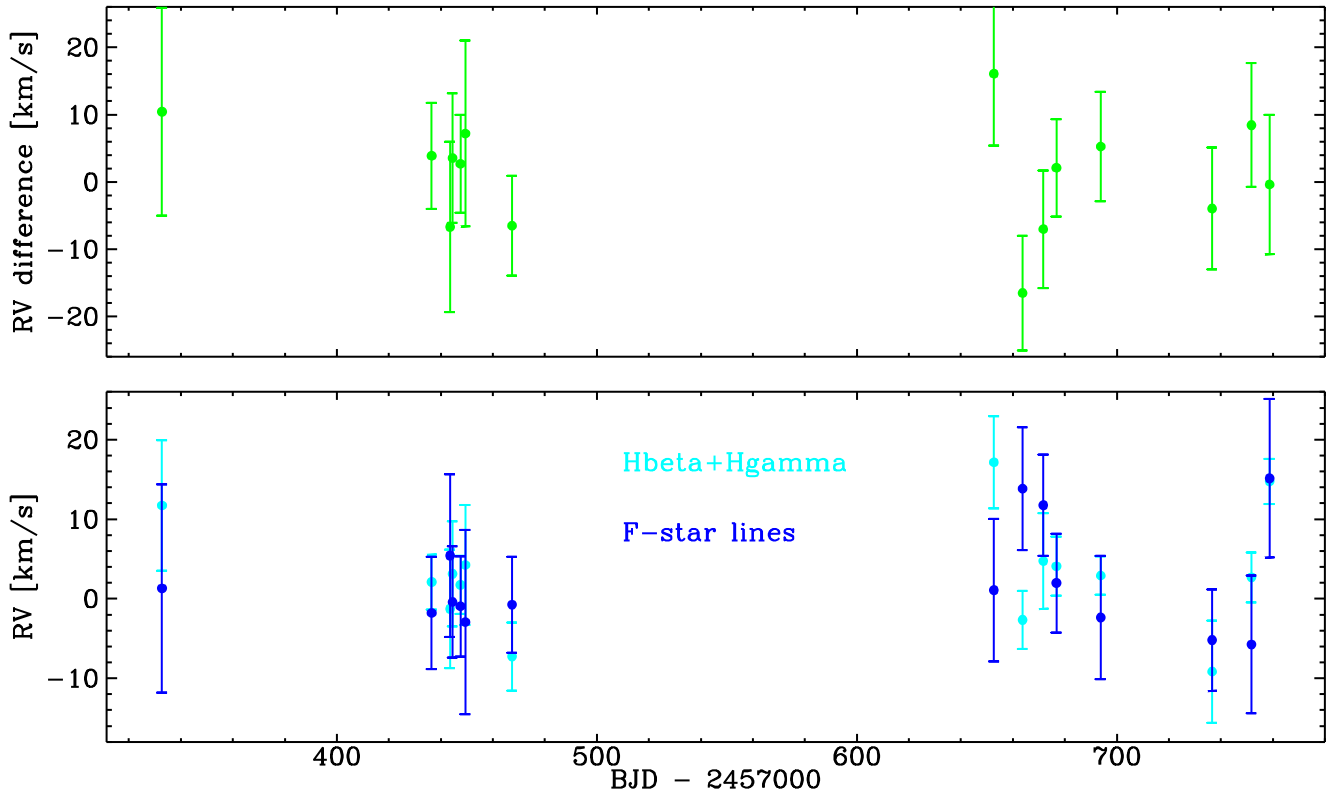
Figure 12. Radial velocities of J08200. The bottom panel shows the velocities determined separately for the sdB (from H β and H γ) and the F companion only (from narrow lines). The top panel shows the difference of these two sets.

In Fig. 13, we show the spectrum of J08200 corrected for instrumental response with two model spectra and their sum overplotted. The sdB model is that of a pure H+He NLTE spectrum with $T_{eff} = 36000$, $\log g = 6.0$, and $\log(N_{He}/N_{H}) = -1.3$ from the grid of Stroeer et al. (2007). The F-star model is one with $T_{eff} = 6800$, $\log g = 4.0$, and $[M/H] = -0.5$ from the grid of Munari et al. (2005). No fitting was attempted in order to produce this solution as there are too many degeneracies. With absolute photometry from *GAIA*, constraints from distance and the spectral energy distribution will make a reliable decomposition possible.

4.3 LB 378

Nineteen 900 s and one 1500 s spectra of LB 378 were obtained between 2016 January and 2017 April. The spectra have S/N ranging from 25 to 81.

Radial velocities for LB 378 were determined using the H β, H β, H γ, H δ, H ζ, and H η lines. For the cross-correlation the average of all CCD#14 spectra was used as a template. The RV results are plotted with large symbols in Fig. 14. An appropriate model was used to measure an absolute RV of $156 \pm 14\,\mathrm{km\,s^{-1}}$.

The spectrum of LB 378 is clearly composite and in fact our spectral decomposition points to a secondary of spectral type F6. Fig. 15 shows that the F star contributes much less to the Balmer lines than the subdwarf. Nevertheless in order to check this, we also determined the RVs based on the four strongest helium lines in the spectrum (λ 4026, 4471, 4686, 4921 Å), which according to the spectral decomposition originate solely in the subdwarf. These RV values are overplotted in Fig. 14 with small symbols, and as they follow the trend of the Balmer-line RVs they confirm that for this

binary the Balmer lines can be used for RV determination of the subdwarf.

The RV curve shows a tentative long-term variation, which is expected for sdB+F/G type binaries (see Vos 2015). Assuming a circular orbit, we fit a RV-amplitude of $K = 12.5(2.3)$ for an uncertain orbital period of $P = 635(146)$. We achieve an RMS = $10.1\,\mathrm{km\,s^{-1}}$ for this fit, and show the fit in Fig. 14. This RMS is typical for what we achieve with the spectroscopic instrumentation used, and is much smaller than the RMS of the RV data of $15\,\mathrm{km\,s^{-1}}$. The RV data do not constrain a meaningful eccentric orbit.

The orbital RV-amplitude and period constrain the mass of the F-star to larger than $M_2 = 0.49\,\mathrm{M_\odot}$, assuming the canonical sdB mass of $0.47\,\mathrm{M_\odot}$. If we assume a typical F star mass of $1.2\,\mathrm{M_\odot}$, the orbital inclination should be $36°$. However, the RV data allow also a longer orbital period, and in that case the inclination will be higher for similar companion masses as assumed above.

The NOT spectra obtained of LB 378 covers only the blue part of the spectrum, but the BOSS spectrum covers the whole optical range and is provided with a reasonable flux calibration, and so we attempted to make a similar by-eye decomposition as for J08200. However, no combination of parameters were found that could reproduce the slope of the combined spectrum to our satisfaction. The models plotted in Fig. 15 are from the same grids as for J08200 but with $T_{eff} = 32000\,K$, $\log g = 5.8$ and $\log(N_{He}/N_{H}) = -1.5$ for the sdB star, and $T_{eff} = 6400$, $\log g = 4.0$ and $[M/H] = -1.0$ for the F star. A summary of these properties is listed in Table 6.

5 RESULTS AND DISCUSSION

During *K2*'s Campaign 5, we discovered six new pulsating hot subdwarf stars. Two have already been published (Baran et al. 2017;
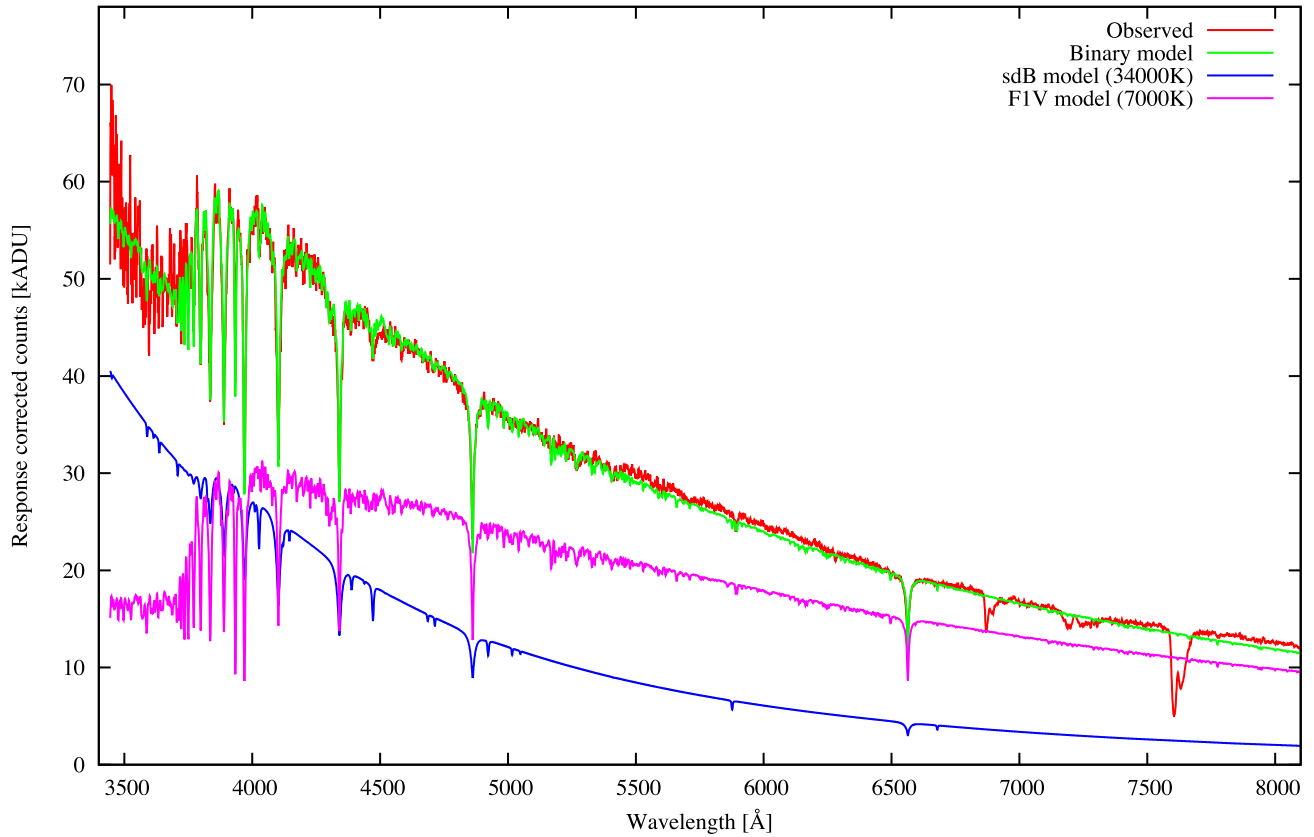
Figure 13. Deconvolved composite spectrum of J08200. Observed and model spectra are labelled in the figure.
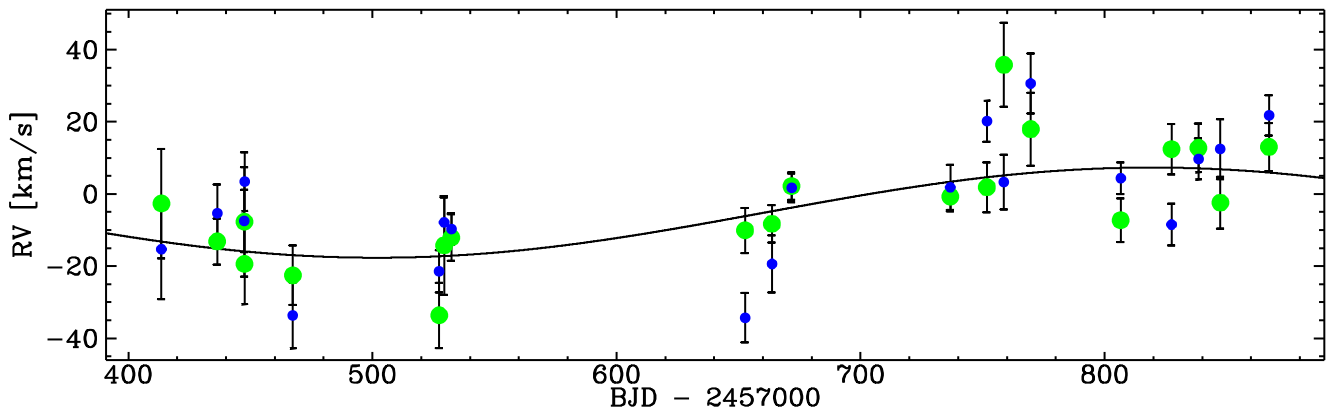

Figure 14. Radial velocities of LB 378. Solid line is the fit.

Jeffery et al. 2017), one is being analysed, and the remaining three are the subject of this paper. We discovered J08360 to be a new *g*-mode sdBV star with a WD companion in a short period orbit of 3.1 d. We also discovered J08200 and LB 378 to be *p*-mode sdBV stars in binaries with main-sequence companions. The nature of these three stars is an interesting brace of properties.

From follow-up spectroscopy, J08360 was discovered to be in a short-period binary with a WD companion. Using canonical masses for the sdB and WD stars, the inclination of the 3.1 d orbit would be 52°, which is well suited for detecting pulsation multiplets. If tidally locked, the multiplet would have $\ell = 1$ splittings of 1.8 μHz, but the only possible multiplet has a splitting of 0.97 ± 0.002 μHz. This would give a rotation period of 50 or 100 d, depending on how the multiplet is interpreted, but in either case, the star is spinning

subsynchronously, and so is not tidally locked to its WD companion. A total of 10 periodicities were detected and all identified as $\ell = 1$ or 2 from *g*-mode asymptotic sequences. We fitted those sequences with solutions of 227.05 ± 0.56 and 131.13 ± 0.14 s, for $\ell = 1$ and 2, respectively. An interesting aspect of J08360's pulsations is that 7 of the 10 periodicities (4 of 6 overtones) occur where the $\ell = 1$ and 2 sequences overlap in period. Is this overlap responsible for driving the pulsations to observable levels? Is there an intrinsic cause or just chance overlap? The answers to such questions are very model-dependent, which is beyond the scope of this paper, and so we are just positing the questions. We note that the other *K2* pulsators do not show a propensity of overlap modes (Reed et al. 2016; Baran et al. 2017; Ketzer et al. 2017), so this feature could just be chance.
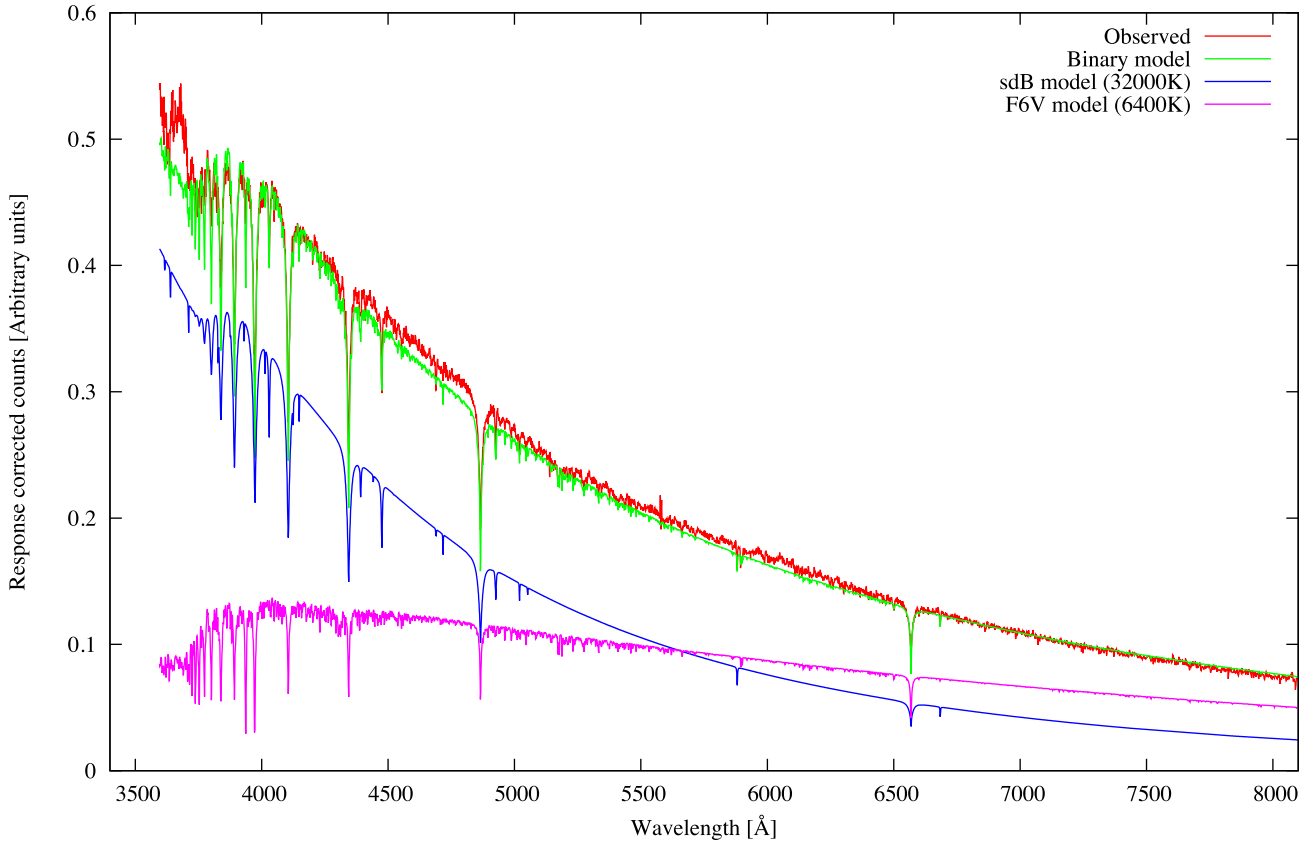
Figure 15. Deconvolved composite spectrum of LB 378. Observed and model spectra are labelled.

Table 6. Summary of spectroscopic and binary properties of LB 378.

Property	Value	Comments
T_{eff} (sdB)	32 000 K	By-eye spectral decomposition
$\log g$ (sdB)	5.8 dex	By-eye spectral decomposition
$\log(n(\mathrm{He})/n(\mathrm{H}))$ (sdB)	-1.5 dex	By-eye spectral decomposition
T_{eff} (MS)	6400 K	By-eye spectral decomposition
$\log g$ (MS)	4.0 dex	By-eye spectral decomposition
Period	635 (146)	RVs, circular orbit
K	12.5 (2.3) km s^{-1}	RVs, circular orbit
Reduced χ^2 of the fit	1.76	RVs, circular orbit
Fit RMS	10.3 km s^{-1}	RVs, circular orbit
$i_{\mathrm{canonical}}$	36°	$M_{\mathrm{sdB}} = 0.47\,\mathrm{M}_\odot$, $M_{\mathrm{F}} = 1.2\,\mathrm{M}_\odot$

J08200 and LB 378 are both *p*-mode pulsators in binaries with F companions. Extracting the pulsations were challenging as pulsations appeared on both sides of the Nyquist frequency. We examined methods for distinguishing between intrinsically super- and sub-Nyquist pulsations in *K2* data sets. While the observed pulsations have variable amplitudes and phases, we have distinguished the difference, to the best of our ability. J08200 has a mixture of sub- and super-Nyquist frequencies, while LB 378 has only intrinsically sub-Nyquist frequencies. Both also show indications of rotationally induced multiplets. For J08200, our best interpretation provides a splitting of $1.01 \pm 0.08\,\mu$Hz, which would be a rotation period (assuming a zero-value Ledoux constant) of 11.5 ± 0.8 d. This would make it a relatively fast sdBV rotator (see Table 2 of Reed et al. 2014). LB 378 has splittings of $0.54 \pm 0.01\,\mu$Hz, which is a

rotation period of 21.5 ± 0.6 d. For both J08200 and LB 378, the multiplets appear in a narrow frequency range, and so cannot be used to test *p*-mode overtone spacings.

We are beginning to see interesting patterns between rotation, pulsation, and binarity. J08200 and LB 378 are the first *K1*-observed sdBV+MS F-K stars and both are *p*-mode pulsators. We have yet to observe an sdBV+MS F-K *g*-mode pulsator. As we continue to process and analyse *K1* and *K2* data, we hope a statistically significant sample of composite systems will allow pulsation–binarity relationships to become clear. One aide will be *GAIA* data (Lindegren et al. 2016). *GAIA* should provide distances and absolute photometry for disentangling fluxes of the sdB+MS systems and will also be able to produce periods from several years of spectroscopy

REFERENCES

Aerts C., Christensen-Dalsgaard J., Kurtz D. W., 2010, Asteroseismology. Springer-Verlag, Berlin
Baran A. S., Winans A., 2012, Acta Astron., 62, 343
Baran A. S. et al., 2012, MNRAS, 424, 2686
Baran A. S., Reed M. D., Østensen R. H., Telting J. H., Jeffery C. S., 2017, A&A, 597, A95
Bevington P. R., Robinson D. K., 2003, Data Reduction and Error Analysis for the Physical Sciences. McGraw-Hill, New York
Carter P. J. et al., 2013, MNRAS, 429, 2143
Charpinet S., Fontaine G., Brassard P., Dorman B., 2000, ApJS, 131, 223
Dawson K. S. et al., 2013, AJ, 145, 10
Deca J. et al., 2012, MNRAS, 421, 2798
Foster H. M., Reed M. D., Telting J. H., Østensen R. H., Baran A. S., 2015, ApJ, 805, 94
Geier S. et al., 2012, in Kilkenny D., Jeffery C. S., Koen C., eds, ASP Conf. Ser. Vol. 452, Searching for the Most Massive Companions to Hot Subdwarf Stars in Close Binaries and Finding the Least Massive Ones. Astron. Soc. Pac., San Francisco, p. 129
Green E. M. et al., 2003, ApJ, 583, L31
Han Z., Podsiadlowski P., Maxted P. F. L., Marsh T. R., Ivanova N., 2002, MNRAS, 336, 449
Heber U., 2016, PASP, 128, 082001

Heber U., Reid I. N., Werner K., 1999, A&A, 348, L25
Ivanova N. et al., 2013, A&A Rev., 21, 59
Jeffery C. S. et al., 2017, MNRAS, 465, 3101
Kawaler S. D., Hostler S. R., 2005, ApJ, 621, 432
Kern J. W., Reed M. D., Baran A. S., Østensen R. H., Telting J. H., 2017, MNRAS, 465, 1057
Ketzer L., Reed M. D., Baran A. S., Németh P., Telting J. H., Østensen R. H., Jeffery C. S., 2017, MNRAS, 467, 461
Kilkenny D., Koen C., O'Donoghue D., Stobie R. S., 1997, MNRAS, 285, 640
Lindegren L. et al., 2016, A&A, 595, A4
Lisker T., Heber U., Napiwotzki R., Christlieb N., Han Z., Homeier D., Reimers D., 2005, A&A, 430, 223
Luo Y.-P., Németh P., Liu C., Deng L.-C., Han Z.-W., 2016, ApJ, 818, 202
Moehler S. et al., 2014, A&A, 568, A9
Munari U., Sordo R., Castelli F., Zwitter T., 2005, A&A, 442, 1127
Murphy S. J., Shibahashi H., Kurtz D. W., 2013, MNRAS, 430, 2986
Østensen R. H. et al., 2010a, MNRAS, 408, L51
Østensen R. H. et al., 2010b, MNRAS, 409, 1470
Østensen R. H., Reed M. D., Baran A. S., Telting J. H., 2014, A&A, 564, L14
Pablo H., Kawaler S. D., Green E. M., 2011, ApJ, 740, L47
Pablo H. et al., 2012, MNRAS, 422, 1343
Reed M., Foster H., 2014, in van Grootel V., Green E., Fontaine G., Charpinet S., eds, ASP Conf. Ser. Vol. 481, Precision Observational Asteroseismology Using Kepler Spacecraft Data. Astron. Soc. Pac., San Francisco, p. 45
Reed M. D. et al., 2011, MNRAS, 414, 2885
Reed M. D., Foster H., Telting J. H., Østensen R. H., Farris L. H., Oreiro R., Baran A. S., 2014, MNRAS, 440, 3809
Reed M. D. et al., 2016, MNRAS, 458, 1417
Still M., Barclay T., 2012, Astrophysics Source Code Library, record soft08004S
Stoughton C. et al., 2002, AJ, 123, 485
Stroeer A., Heber U., Lisker T., Napiwotzki R., Dreizler S., Christlieb N., Reimers D., 2007, A&A, 462, 269
Telting J. H. et al., 2012, A&A, 544, A1
Telting J. H., Østensen R. H., Reed M., Farris L., Baran A., Oreiro R., O'Toole S., 2014, in van Grootel V. et al., eds, ASP Conf. Ser. Vol. 481, Low-resolution radial-velocity monitoring of pulsating sdBs in the Kepler Field. Astron. Soc. Pac., San Francisco, p. 287
Vos J., 2015, EAS Publ. Ser. Vol. 71, Eccentricity Pumping Through Circumbinary Disks in Hot Subdwarf Binaries. Cambridge Univ. Press, Cambridge, p. 207
Vos J., Østensen R. H., Vuckovic M., Telting J. H., 2017, A&A, p. in press
Webbink R. F., 1984, ApJ, 277, 355
York D. G. et al., 2000, AJ, 120, 1579

This paper has been typeset from a TEX/LATEX file prepared by the author.